

Brownian Dynamics Simulation of the Growth of Metal Nanocrystal Ensembles on Electrode Surfaces from Solution. I. Instantaneous Nucleation and Diffusion-Controlled Growth

J. L. Fransaeer[†] and R. M. Penner^{*‡}

Department MTM, KULeuven, de Croylaan 2, 3001 Heverlee, Belgium, and Institute for Surface and Interface Science and Department of Chemistry, University of California, Irvine, Irvine, California 92679-2025

Received: February 22, 1999; In Final Form: June 25, 1999

The diffusion-controlled growth of ensembles of metal nanoparticles on a planar surface from solution is modeled using Brownian Dynamics (BD) simulation method. Both random and hexagonal 2D ensembles were considered with coverages ranging from 5×10^9 to 2×10^{11} cm⁻². Attention is focused on the evolution of particle size dispersion as a function of the experimental variables. Three temporal regimes in the growth of these nanoparticle ensembles are distinguished from the simulation data: At short times ($t < 20$ ns), the standard deviation of the particle radius, σ_R , rapidly increases to 0.05–0.1 nm. At intermediate times in the interval from 20 to 200 ns, σ_R peaks and begins to decline—nearly to zero in some simulations. This “convergent” growth segment continues until overlap of the diffusion layers of adjacent nanoparticles on the surface is nearly complete. We derive an analytical expression for σ_R in this time regime which is based on the stochastic nature of the deposition process, and excellent agreement with the simulation data is obtained. Finally, at yet longer times (at which diffusion to the surface is planar), the behavior of random and hexagonal ensembles diverge: Random ensembles again transition into a divergent growth regime in which σ_R increases monotonically with time; the size dispersion of hexagonal arrays, however, continues to decrease with deposition time. In this time regime, the data support the conclusion that size dispersion is caused by an inhomogeneous distribution of interparticle distances which translates into an inhomogeneity in the diffusion-limited flux at each particle.

I. Introduction

Physical vapor deposition techniques (PVD) have been used to prepare supported particles for fundamental investigations of their properties in catalysis, in surface-enhanced Raman spectroscopy (SERS), etc.^{1,2} However, PVD is limited in terms of the number of different metals which may be deposited as nanoparticles, and it has proven to be difficult to obtain nanoparticles smaller than 20 Å in diameter using this method. A desire to overcome these two deficiencies provides the motivation to develop an electrochemical route to size monodisperse metal nanoparticles. Electrochemistry provides a means by which many metals and alloys can be deposited onto a conductive surface from an electrolyte. In this sense, electrochemistry is extremely versatile. On the other hand, it has not been possible to exert control over the dimensional uniformity³ of electrodeposited metal structures. In particular, meso-scale⁴ metal particles have been obtained by electrochemical deposition; however, the relative standard deviation of the particle diameter ($RSD_{\text{dia.}} = \langle \text{dia.} \rangle / \sigma_{\text{dia.}}$) has been 20–50%^{5–7} in the best cases reported to date. In the next paragraph we shall summarize the current understanding of particle growth on surfaces as it applies to the growth of particles by PVD. We will conclude that our inability to obtain size monodisperse metal particles by electrochemical deposition is surprising. Thus, it is useful to ask the question, What makes PVD particle growth different

from electrochemical particle growth? or more generally, What factors are responsible for the development of size dispersion in ensembles of metal particles grown by electrodeposition? We attempt to answer these questions in this paper.

The issue of particle size dispersion in the growth of particles on surfaces using PVD was addressed by Ngo and Williams.⁸ These workers concluded that temporally discrete nucleation⁹ leads to very narrow particle size distributions for any growth duration, and irrespective of the rate law which applies (e.g., particle radius, $r^n \propto t$ where $n = 2, 3$, and 4),⁸ provided every particle on the surface grows in accordance with the *same* rate law. Temporally discrete nucleation is also a requirement for growing size monodisperse colloidal particles in solution.^{10–12} At the end of the nucleation phase, the $RSD_{\text{dia.}}$ is predicted to decrease as a function of time for virtually any rate law.⁸ The size monodispersity for nanoparticles growing on a surface will be improved by manipulating the growth conditions as follows:⁸ (1) The flux of monomer to the surface during growth should be high (to rapidly saturate defect sites in order that nucleation ends as quickly as possible); (2) the sample temperature should be low (since the growth rate for particles will depend on the diffusion coefficient for surface-adsorbed monomer, which will be inversely related to the surface temperature. By decreasing the particle growth rate, it is hoped that islands will be prevented from interacting with one another via the depletion of surface monomer); and (3) the nucleation density of the surface should be as low as possible (again, so that the growth of neighboring particles is decoupled). Although Ngo and Williams⁸ were

* Address correspondence to: rmpenner@uci.edu.

[†] KULeuven.

[‡] Institute for Surface and Interface Science and University of California.

considering the growth of particles from a gas phase flux of monomers, these principles should also apply to electrochemical growth.

Temporally discrete nucleation has also been observed for the electrochemical deposition of silver⁶ and platinum⁵ nanoparticles on graphite. Nanoparticles of these two metals ($10^8 - 10^{10}$ nanoparticles cm^{-2}) were obtained using a potentiostatic pulse having a duration of 5–100 ms and a large deposition overpotential, $|E_{\text{appl}} - E'_{\text{M}+/ \text{Mo}}|$, of 300–500 mV. Measurements of the particle nucleation density and diameter for depositions of different durations provided strong evidence for instantaneous nucleation¹³ in these experiments. However, on the graphite surfaces on which these syntheses are conducted, the expected degree of size monodispersity was *not* obtained. Specifically, “small” metal nanocrystals (dia. < 6 nm) possessed moderately good size monodispersity (e.g., for platinum,⁵ $\text{RSD}_{\text{dia.}} \leq 35\%$), however, both the standard deviation and the relative standard deviation *increased* as a function of the deposition time. In other words, nucleation *is* temporally discrete, but particle radii do not converge as a function of growth duration. In the context of the work of Ngo and Williams,⁸ this result is difficult to rationalize. The origin of this paradox, as we shall see, is strong diffusional coupling between neighboring metal particles growing at diffusion control in a solution.

The Brownian dynamics (BD) simulation method can be employed to elucidate the factors that are responsible for size dispersion in the case where particles nucleate instantaneously, grow at a diffusion-controlled rate from solution phase precursors, and are confined during growth to a flat surface. In the BD simulations which we have performed, we have explicitly considered growth durations which are long compared with the interaction time, t_i , between nearest neighbors on the surface:

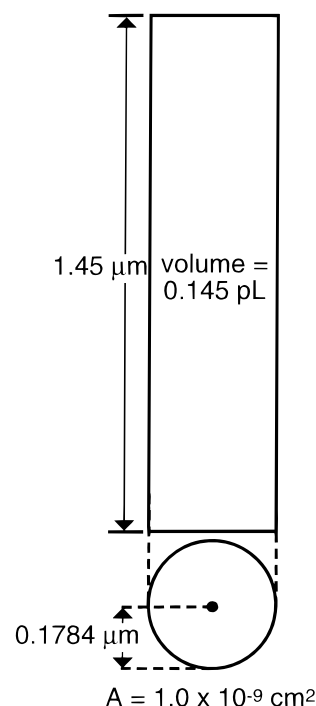
$$t_i = \langle x \rangle^2 / 2D \quad (1)$$

where $\langle x \rangle$ is half the average distance between nearest neighbors on the surface, and D is $1.20 \times 10^{-5} \text{ cm}^2 \text{ s}^{-1}$ (the diffusion coefficient for silver ions in dilute, aqueous electrolytes). The purely diffusive motion of individual ions or molecules is simulated using the algorithm¹⁴

$$\mathbf{r} = \mathbf{r}_0 + (2D\Delta t)^{1/2} \mathbf{R} \quad (2)$$

where \mathbf{r}_0 and \mathbf{r} are the initial and final positions of a particle relative to the time interval, Δt , and \mathbf{R} is a vector of Gaussian random numbers. Compared with simulations based on the explicit finite difference (EFD) approach, developed for electrochemical problems by Feldberg^{15–18} and others, BD has been used much less frequently to model electrochemical processes because it is far less computationally efficient for most problems which interest electrochemists. However, BD has occasionally been used to model electrochemical phenomena in experiments involving complex electrode geometries. Examples include the transport of ions between microband electrodes¹⁹ and the transport of ions²⁰ and molecules²¹ between a hemispherical scanning probe microscope tip and a planar electrode surface. A second category of problems that are conveniently approached using BD are those which probe stochastic processes. Nagy and Denault²² recently used BD to model the diffusion-controlled growth of square arrays of metal nanoparticles. In that work, the growth of a single metal particle was modeled in 3D using periodic boundary conditions that simulated a square particle array;²² the size dispersion of an *ensemble* of interacting particles was therefore not addressed. In the simulations described here,

SCHEME 1



ensembles of metal particles were grown in a much larger simulation volume under diffusion control from single atoms to mean diameters of up to 3 nm from a 10^{-3} M “solution” of metal ions. Each metal particle in these ensembles was explicitly modeled so that the development of size dispersion for the ensemble could be monitored as a function of the deposition time. The behaviors of “random” ensembles of nanoparticles and hexagonal arrays are compared across a range of experimentally relevant nucleation densities.

We shall also discuss recently developed analytical models for the growth of ensembles of particles on surfaces. This problem has attracted the interest of several theoreticians and analytical equations that describe the reaction rate as a function of the experimental parameters were developed by Fletcher and co-workers (e.g., ref 23) (for the case where adjacent nanoparticles grow independently from one another) and Scharifker and co-workers (e.g., ref 24) (for the strong interaction case that is of interest here). We compare the BD simulation results with the predictions of Scharifker and co-workers below.

II. The BD Simulation Method

Our 3D BD simulations are intended to model the diffusion-controlled growth of nanoscopic silver hemispheres on a graphite surface following an instantaneous nucleation event. We have neglected the possible contributions due to electromigration or diffusiomigration of the silver ions in solution. In this paper, we refer to these hemispheres as nanoparticles or nuclei. The algorithm of McCammon was used except that the Gaussian vector in eq 1 was replaced with a 32-bit number uniform in the interval from -1 to 1 . A time step, Δt , of 80 ps was chosen. In addition, to achieve the needed diffusion coefficient of $1.20 \times 10^{-5} \text{ cm}^2 \text{ sec}^{-1}$, a multiplicative scaling factor was employed. This modification permitted the use of a fast random number generator, RCARRY,²⁵ having a very long period of approximately 2^{1407} . The dimensions of the cylindrical simulation volume of 0.145 pL are shown in Scheme 1. The surfaces of this cylinder were impermeable, and the simulation volume was filled with approximately 87 320 particles (silver ions) to give

a concentration of 1×10^{-3} M. Initially, the silver ions, which were modeled as points, were uniformly distributed within the simulation volume. Computational speed was increased by allowing silver ions initially (i.e., at $t = 0$) located at a distance, z , from the electrode surface to remain motionless until $t_c = z^2/2.5D$. Each simulation of 0.5 ms required approximately 10 days on a DEC Alpha 21064 workstation.

A number of metal nuclei were arranged either randomly or in a hexagonal array (see below) on the electrode surface at the beginning of each simulation. These nuclei consisted initially of a single silver atom which was modeled as a hemisphere of radius = 0.2 nm. These nuclei were stationary throughout the simulation. During the simulation, the collision of a diffusing silver ion with any of the nuclei on the electrode surface resulted in all of the following: (1) The removal of that ion from the simulation; (2) the incremental growth of the hemispherical nucleus involved in the collision by a volume equal to that of a single silver atom; and (3) the addition of an electron to the tally for that simulation time increment. The formation of metal adatoms (e.g., by discharge of silver ions on the electrode surface away from nuclei) was not permitted. This boundary condition at $z = 0$ closely models the behavior of highly oriented pyrolytic graphite in our experiments.

The reliability of our algorithm for modeling electrochemical phenomena was verified by comparing simulated potential step chronocoulometry and chronoamperometry experiments with analytical expressions describing these current or charge transients. These comparisons were carried out for the case where the electrolyzed form of the redox couple was soluble, and the electrode geometry was either planar or hemispherical. In each of these cases (data not shown), excellent agreement of the simulated transients with calculated transients was obtained. The diffusion-controlled growth of single silver nuclei, located in the center of the electrode shown in Scheme 1, was also simulated. Figure 1 shows a current–time transient (Figure 1a), and a plot of the radius versus time (Figure 1b). The simulation results presented in Figure 1 reflect the average of three separate simulations performed using different plating “solutions” (different initial positions for the silver ions in the solution). The solid line shown in Figure 1 is the prediction of eq 3 that is the analytically exact solution to the problem of time-dependent growth of a single hemispherical nucleus:²⁶

$$i(t) = \frac{\pi F(2D_{\text{Ag}^+} C_{\text{Ag}^+}^*)^{3/2} (M_{\text{Ag}} t)^{1/2}}{\rho_{\text{Ag}}^{1/2}} \quad (3)$$

Here D_{Ag^+} is the diffusion coefficient (1.2×10^{-5} cm² s⁻¹), $C_{\text{Ag}^+}^*$ is the concentration of silver ions (1.0×10^{-6} moles cm⁻³), M_{Ag} is the atomic weight of silver (107.87 g mole⁻¹), and ρ_{Ag} is its density (10.5 g. cm⁻³). Likewise, the solid line in Figure 1b is that predicted by eq 4:²⁶

$$R(t) = \frac{(2D_{\text{Ag}^+} C_{\text{Ag}^+}^* M_{\text{Ag}} t)^{1/2}}{\rho_{\text{Ag}}^{1/2}} \quad (4)$$

The agreement of the mean simulation current and radius with these equations is very good even at the shortest times. Especially for the current–time plot of Figure 1a, this agreement at short times is at first somewhat surprising. Equation 3 assumes that the concentration of silver ions at the surface of the nuclei is zero, whereas the initial surface concentration of silver ion in the simulation is the bulk concentration (i.e., 1.0 mM). Consequently, a surface concentration of zero must be established at the onset of deposition in the simulation and one

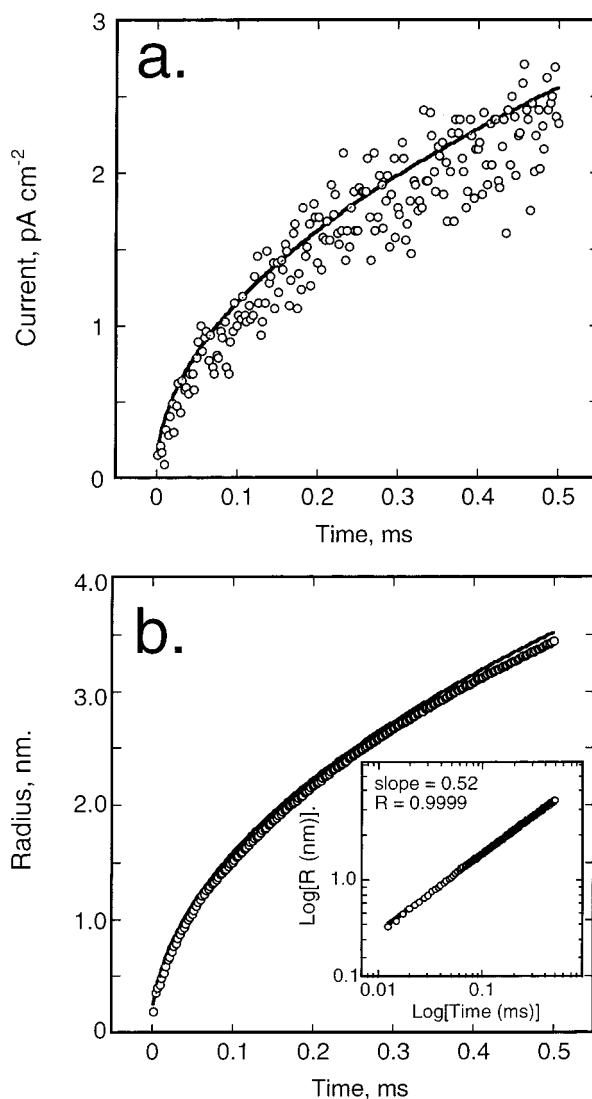


Figure 1. Results of BD simulations of the growth of a single silver particle centered on the electrode shown in Scheme 1. The mean current (a) and radius (b) are plotted as a function of time for three simulations which were carried out using plating solutions with different initial positions of the silver ions. Error bars shown in (a) indicate $\pm 1\sigma$ for the three data sets.

expects intuitively that the simulated current should exceed the prediction of eq 3 in this time domain. This effect is not seen in Figure 1 because metal deposition can only occur on the surface of the nuclei, which at the start of the simulation are very small ($r_{\text{initial}} = 2.0 \times 10^{-8}$ cm, the “radius” of a single silver atom).

Results and Discussion

A. Random Ensembles. Scheme 2 (left column) shows typical nuclei positions for simulations in which the nuclei were randomly positioned on the electrode surface. Six nucleation densities, ranging from 5×10^9 cm⁻² (i.e., 5 nuclei on a 10^{-9} cm² surface) to 2×10^{11} cm⁻² (i.e., 200 nuclei), were investigated. Figure 2 (open circles) shows that the mean nearest neighbor distance ranges from 80 (± 20) nm to 11 (± 6) nm as a function of the nucleation density. In conjunction with the diffusion coefficient ($D = 1.2 \times 10^{-5}$ cm² s⁻¹), these nearest neighbor distances translate into interaction times (defined as $\tau = x^2/2D$, where x is half of the nearest neighbor distance), ranging from 0.1 to 1 μ s. In other words, the growth of

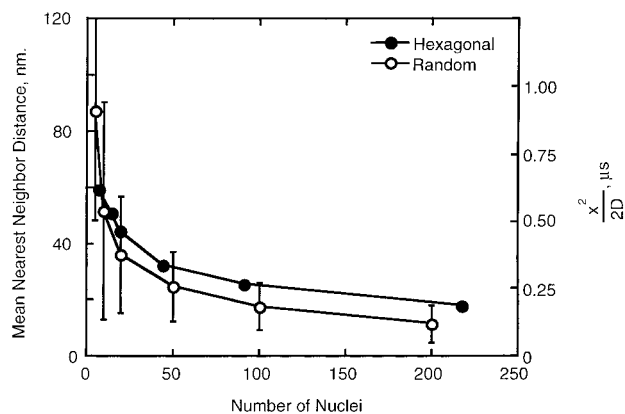
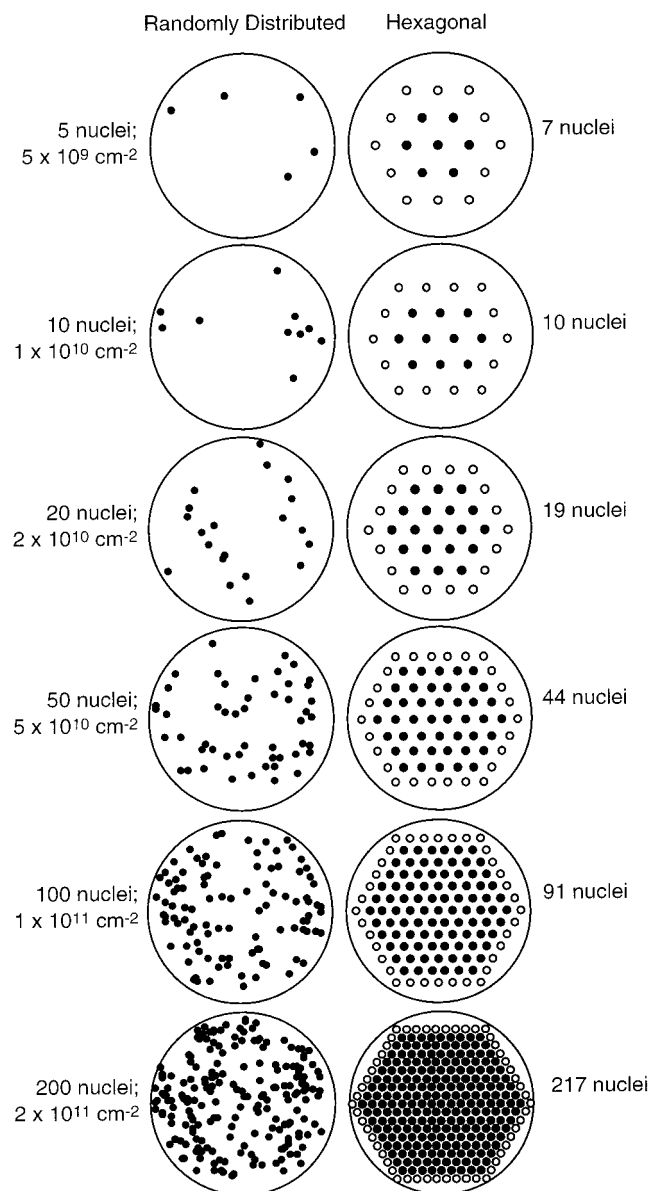


Figure 2. Calculation of the mean nearest neighbor distance, and the interaction time (right axis) as a function of the number of nuclei on the electrode surface. Error bars on the data points for the random ensembles are $\pm 1\sigma$ for the dispersion of the distance and time about the mean value.

SCHEME 2



individual nuclei on the surface will be diffusionally coupled to that of neighboring nuclei virtually from the onset of the 500 μs simulation. We therefore expect the growth rate for

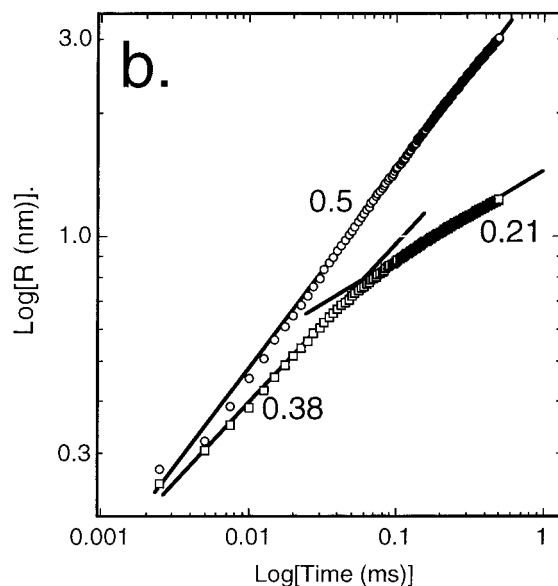
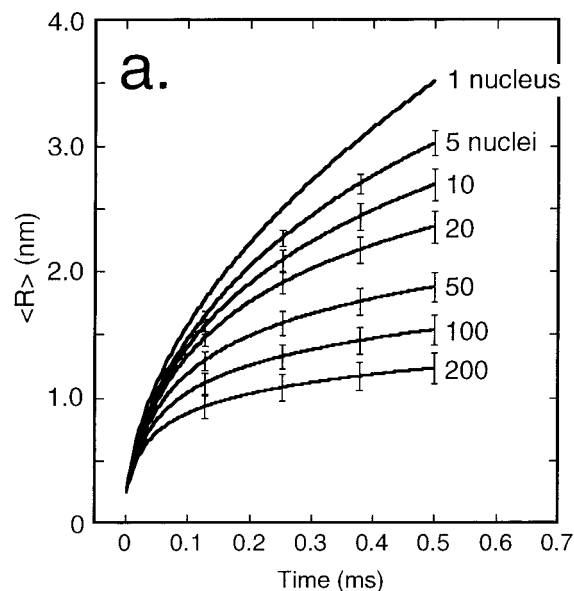


Figure 3. (a) Plots of the mean radius, $\langle R \rangle$, versus time for the growth of random ensembles having six different nucleation densities, and for one particle. Individual traces are labeled with the nucleation density in units of 10^9 cm^{-2} . (b) Plots of $\log(R)$ vs $\log(t)$ for the single particle growth experiments and for the most densely nucleated surface (labeled “200” in (a)). The linear behavior of the isolated particle is consistent with the predictions of eq 4, whereas multiple, coupled nuclei do not grow in accordance with a power law.

individual nuclei to be significantly lower than that seen for a single nucleus in Figure 1, and the mean growth rate to decrease with increasing nucleation density.

The growth curves shown in Figure 3 reveal that these expectations are realized. In this figure, the mean radius, $\langle R \rangle$, is plotted as a function of time for random nuclei at six nucleation densities and for a single nucleus. As in Figure 1, the data for each nucleation density represent the average of three simulations. The error bars track the standard deviation of the nanoparticle radii, $\pm 1\sigma_R$, at five times. After 20 μs , the seven growth curves diverge and the growth rate decreases with increasing nucleation density. In contrast to the situation for a single metal nucleus (where $r \propto t^{1/2}$), however, the dependence of $\langle R \rangle$ on time is not described by a simple power law for any of the surfaces supporting multiple nuclei. This fact is worth noting because a power law has often been employed in previous

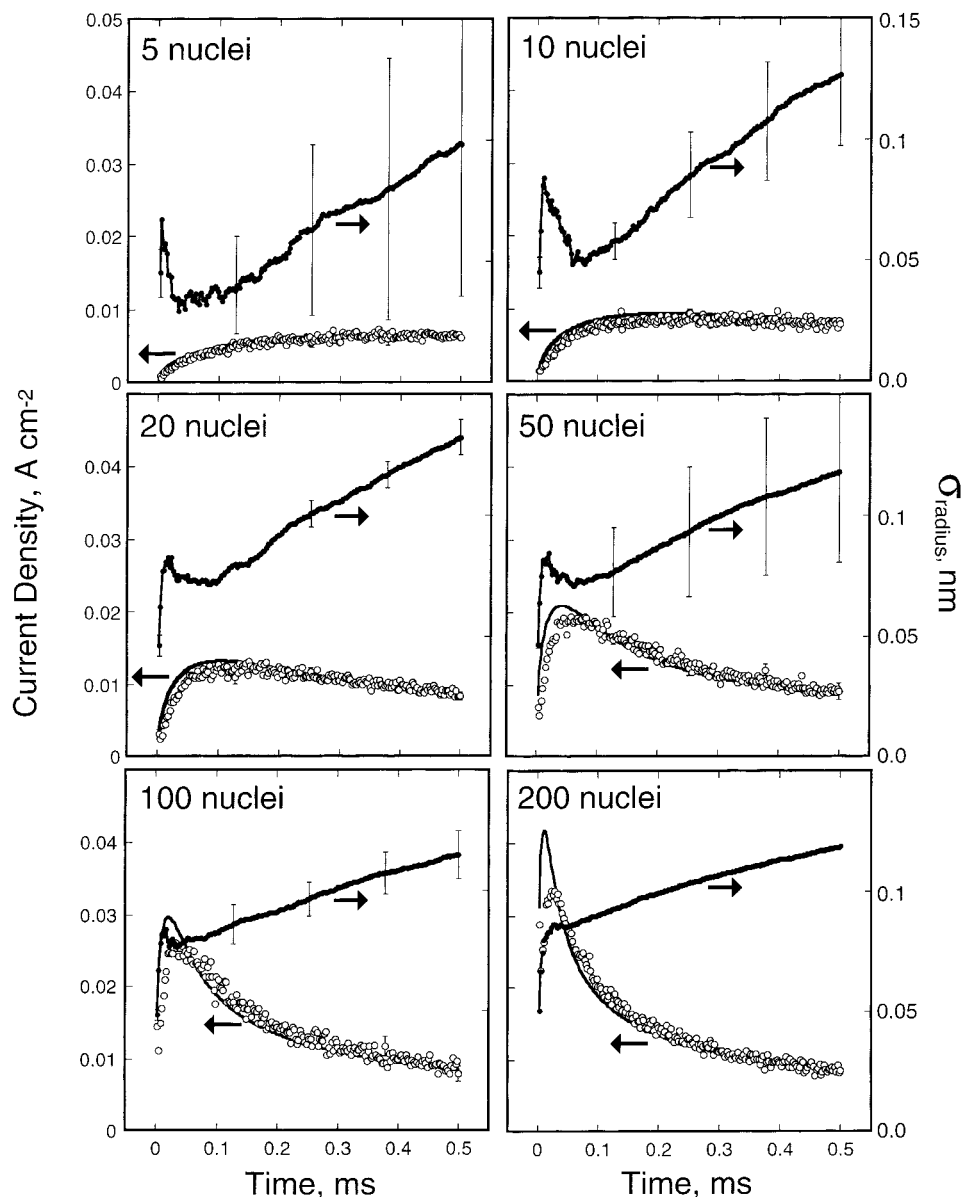


Figure 4. Current density (open circles) and the standard deviation of the particle radius, σ_R , (solid circles) as a function of time for *random ensembles* at six nucleation densities. These BD simulation results represent the mean of three simulations, each of which involved a different silver plating solution, and different positions for nuclei on the surface. The standard deviation of the current and σ_R are indicated by the error bars ($\pm 1\sigma$) which are shown at five times. Data sets are labeled with the nucleation density in units of 10^9 cm^{-2} .

studies to describe the growth of nanoparticles from the gas phase. For the 200 nuclei surface, for example, Figure 3b shows that the dependence of $\langle R \rangle$ on time is approximately $\langle R \rangle \propto t^{0.4}$ for $t < 0.04 \text{ ms}$, and approximately $\langle R \rangle \propto t^{0.2}$ for $0.1 \text{ ms} < t < 0.5 \text{ ms}$. In the paragraphs that follow, attention is focused on the time evolution of the current and the size dispersion of these nanoparticles.

In Figure 4, the current density, j , and σ_R are plotted as a function of time for the six random ensembles. In these plots, the current density is defined as the total current divided by the geometric area of the surface (i.e., 10^{-9} cm^{-2}). An increasing current density is initially observed for all six ensembles, qualitatively as predicted for noninteracting nuclei by eq 3, however, the current per nucleus is smaller than that predicted by eq 3. Eventually, the hemispherical diffusion fields of adjacent nuclei on the surface merge to form an approximately planar diffusion field and a transition is observed from an increasing current, to a current density that decays as $t^{-1/2}$. This functionality for the current is expected for a reaction occurring

at the planar diffusion-controlled rate.²⁷ As seen in Figure 4, the transition time indicated by the current peak, t_{peak} , becomes smaller as the nucleation density and the proximity of the nuclei on the surface to one another increases.

An analytical expression for the current in the case where nucleation is spatially random and instantaneous was derived by Scharifker and Hills in 1983:²⁴

$$j(t) = \frac{zFD_{\text{Ag}^+}^{1/2}C_{\text{Ag}^+}^*}{\pi^{1/2}t^{1/2}} [1 - \exp(-N_0\pi kD^{1/2}t)] \quad (5)$$

where $j(t)$ is the current normalized by the geometric area of the surface (A cm^{-2}), N_0 is the nucleation density (cm^{-2}), and k is a dimensionless constant given by

$$k = \sqrt{\frac{8\pi C_{\text{Ag}^+}^* M_{\text{Ag}}}{\rho_{\text{Ag}}}} \quad (6)$$

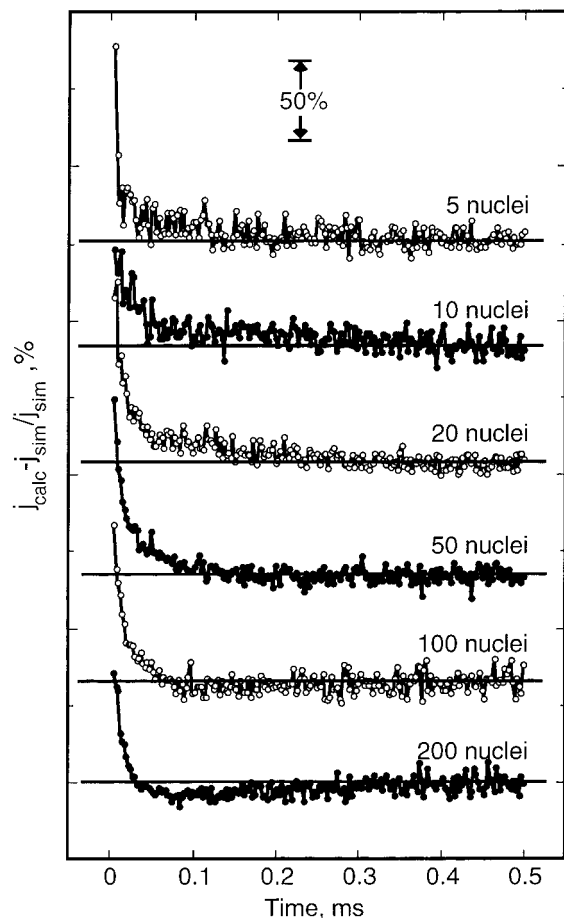


Figure 5. Residual current, plotted as the percentage of the simulation current, for the predictions of eq 5. The agreement of this analytical equation for the current derived by Scharifker et al.¹⁵ with the BD results is excellent except at the shortest times.

For each of the data sets shown in Figure 4, the predictions of eq 5 are plotted as a solid line. Figure 5 shows that the $j(t)$ calculated from eq 5 tends to be somewhat higher than the simulation $j(t)$ for the first 10–20 μs of the deposition independent of the nucleation density; however, for all later times this disparity is less than 10%. No disagreement in the t_{peak} value is seen within the reproducibility of the simulation results.

The solid circles in Figure 4 trace the evolution of the standard deviation of the particle radius, σ_R , as a function of deposition time. Error bars indicate the standard deviation of σ_R that was calculated for the three simulations comprising the data set for each nucleation density. For all six nucleation densities, a rapid increase in the size dispersion is seen during the first 10–20 μs of growth culminating in a standard deviation of 0.05–0.1 nm \pm 0.02 nm. Then a time interval was observed during which σ_R decreased by 2–40%. This “convergent growth” regime continues nearly until t_{peak} , at which point σ_R again increases monotonically to 0.1–0.15 nm during the remainder of the simulation.

The simulation data of Figure 4 predicts that the size monodispersity of a metal nanocrystal ensemble growing under diffusion control will degrade as a function of time provided the total plating duration is much longer than t_{peak} . This is exactly what has been seen experimentally for the growth of silver⁶ and platinum⁵ nanocrystals on graphite surfaces, and for the growth of silver nanocrystals on Si(100).⁷ The nucleation densities for metal nanoparticles on graphite and silicon are near the bottom of the range explored here ($\sim 10^{-9}$ cm⁻²), whereas

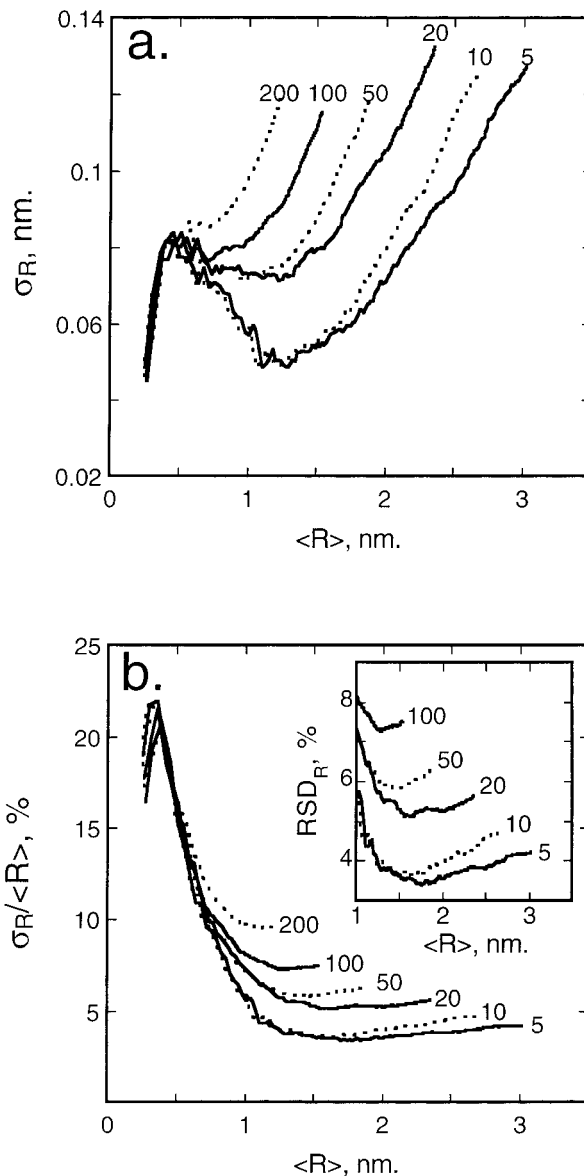


Figure 6. Plots of σ_R (a) and $\sigma_R / \langle R \rangle$ (b) as a function of $\langle R \rangle$ for the simulation data of Figure 4 (i.e., random ensembles). Both σ_R and $\sigma_R / \langle R \rangle$ (see inset) increase as a function of time following the overlap of diffusion layers for adjacent nuclei on the surface.

the metal ion concentration and diffusion coefficient are essentially the same. Consequently, t_{peak} is 0.5–1.0 ms while the typical plating pulse durations necessary to grow nanoparticles having radii of 1–20 nm range from 10 to 200 ms.^{5–7} On the basis of the results of Figure 4, the metal nanoparticles in these experiments are growing in the divergent time domain, $t > t_{\text{peak}}$, for more than 90% of the duration of the potentiostatic growth pulse.

In Figure 4, the nucleation density appears to have little effect on the size monodispersity of metal nanoparticles because in each simulation, the final σ_R value at 0.5 ms is near 0.1 nm. This conclusion is incorrect. Instead, the size monodispersity for particles having a particular mean radius $\langle R \rangle$ improves dramatically with decreasing nucleation density—exactly as predicted by Ngo and Williams.⁸ This trend is apparent in Figure 6 where σ_R and $\sigma_R / \langle R \rangle$ have been plotted versus $\langle R \rangle$ instead of versus deposition time. For $\langle R \rangle = 2.0$ nm, for example, $\sigma_R = 0.06$ nm for the least densely nucleated surface (5×10^9 cm⁻²), whereas $\sigma_R = 0.12$ nm is seen for a nucleation density just an order of magnitude higher. What is the mechanism of this size

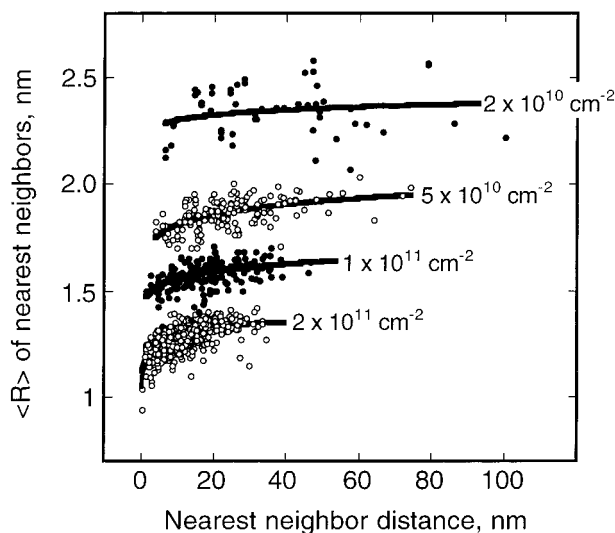


Figure 7. Plots of the mean radius, $\langle R \rangle$, for nearest neighbors as a function of the nearest neighbor distance for four random ensembles. Solid lines represent the least-squares fit of an equation of the form: $y = ax^b + c$ to each data set. Each data set is labeled with the nucleation density.

distribution broadening? Following t_{peak} , the diffusion layer is approximately planar across the entire electrode surface and the flux of metal ions per unit area on the surface is spatially uniform. Nuclei are randomly located on the surface, however, and the nucleation density is locally variable. Densely nucleated areas can therefore be expected to grow more slowly than regions of the same size (and sharing the same planar flux) but encompassing a smaller number of nanoparticles. This mechanism should lead to a recognizable correlation between the mean radius of nearest neighbors on the surface and the distance separating them: Figure 7 shows that this is indeed the case for the four highest nucleation densities we have investigated. In Figure 7, plots of the mean radius versus interparticle distance have been fit with a polynomial of the form $y = ax^b + c$ and the coefficient a is positive in all cases. A second independent check on this explanation is provided by BD simulations of hexagonal arrays of growing nanoparticles in which the nearest neighbor distance for every particle on the surface is identical, and the mechanism of size distribution broadening mentioned above cannot operate. We discuss these simulations below.

An unexpected and somewhat surprising correlation is also seen for the *difference* in radius between two nearest neighbors, and the distance separating them. As shown in Figure 8, as the distance between two neighbors decreases (and $\langle R \rangle$ for these two particles decreases), the difference in radius actually increases! Schematically, the situation is as depicted at the bottom of Figure 8. It is apparent that the division of flux between two nearest neighbors is less and less equitable as the distance between them decreases, with the larger of the two receiving a disproportionate fraction of the total flux. It is interesting to note that in this “strong coupling” regime, a trend exists for large particles to grow at a faster rate than smaller particles. This trend is exactly the opposite as that predicted by Reiss¹¹ for colloid particles growing in bulk solution.

B. Hexagonal Ensembles. Shown in Figure 9 are BD simulations for the hexagonal arrays of nanoparticles shown in Scheme 1. In each case, a hexagonal domain of nanoparticles (black dots) is surrounded by “guard” nanoparticles (open circles). The purpose of these guard nanoparticles is to eliminate the edge effects at the frontier of the domain. Current density vs time transients are plotted in Figure 9 for the hexagonal

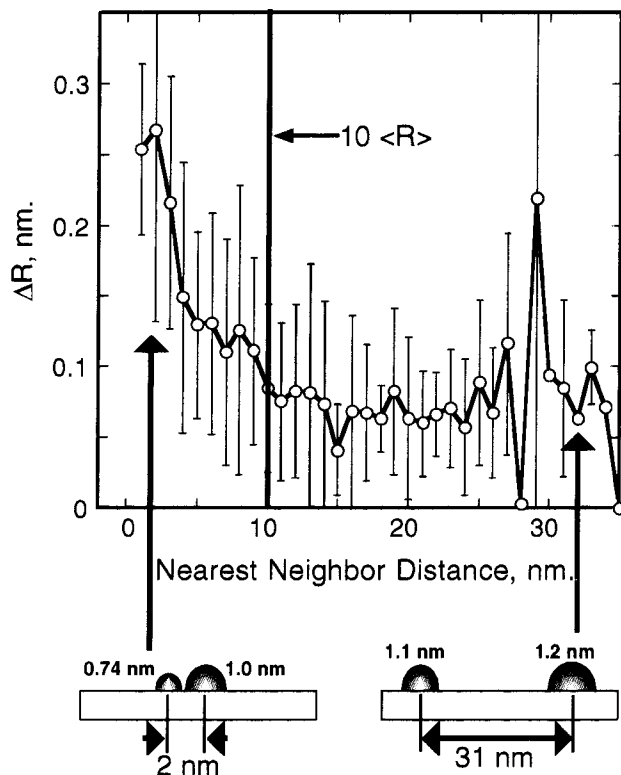


Figure 8. Plot of the difference in radius, ΔR , as a function of the nearest neighbor distance for random ensembles having a nucleation density of $2 \times 10^{11} \text{ cm}^{-2}$. Even as the mean radius of nearest neighbors decreases as shown in Figure 7, the ΔR increases, as shown schematically in the bottom figure.

arrays. As in Figure 4, the current density is defined as the total current measured at all nonguard nuclei divided by the total electrode area of 10^{-9} cm^{-2} . Because guard nuclei occupy some of the available surface area, this means that the current densities calculated in this way are overestimated by 5–10%. The error introduced by this assumption, however, does not affect any of the conclusions derived from the simulation data.

The current–time transients for the hexagonal arrays of Figure 9 are qualitatively similar to those of the random arrays of Figure 4 in that the transients of Figure 9 are also peaked. The origin of this current peak—a transition from locally hemispherical diffusion about each particle to semi-infinite planar diffusion to the entire electrode surface—is also the same for hexagonal arrays. Again, Scharifker²⁸ derived analytical expressions for these transients as follows. At short times, $t < \gamma^{-1}$ (where $\gamma = 2\sqrt{3} N_0 k D$):

$$j(t) = \frac{FD_{\text{Ag}^+}^{1/2} C_{\text{Ag}^+}^*}{(\pi t)^{1/2}} \pi N_0 k D_{\text{Ag}^+} \quad (7)$$

where k is defined as in eq 6. At intermediate times, $\gamma^{-1} \leq t \leq (0.75\gamma)^{-1}$:

$$j(t) = \frac{\sqrt{3}FD_{\text{Ag}^+}^{1/2} C_{\text{Ag}^+}^*}{(\pi t)^{1/2}} \left[\sqrt{\gamma - 1} + \gamma \left(\frac{\pi}{6} - \arctan \sqrt{\gamma - 1} \right) \right] \quad (8)$$

At long times, $t \geq (0.75\gamma)^{-1}$, the current density is Cottrellian:²⁷

$$j(t) = \frac{FD_{\text{Ag}^+}^{1/2} C_{\text{Ag}^+}^*}{(\pi t)^{1/2}} \quad (9)$$

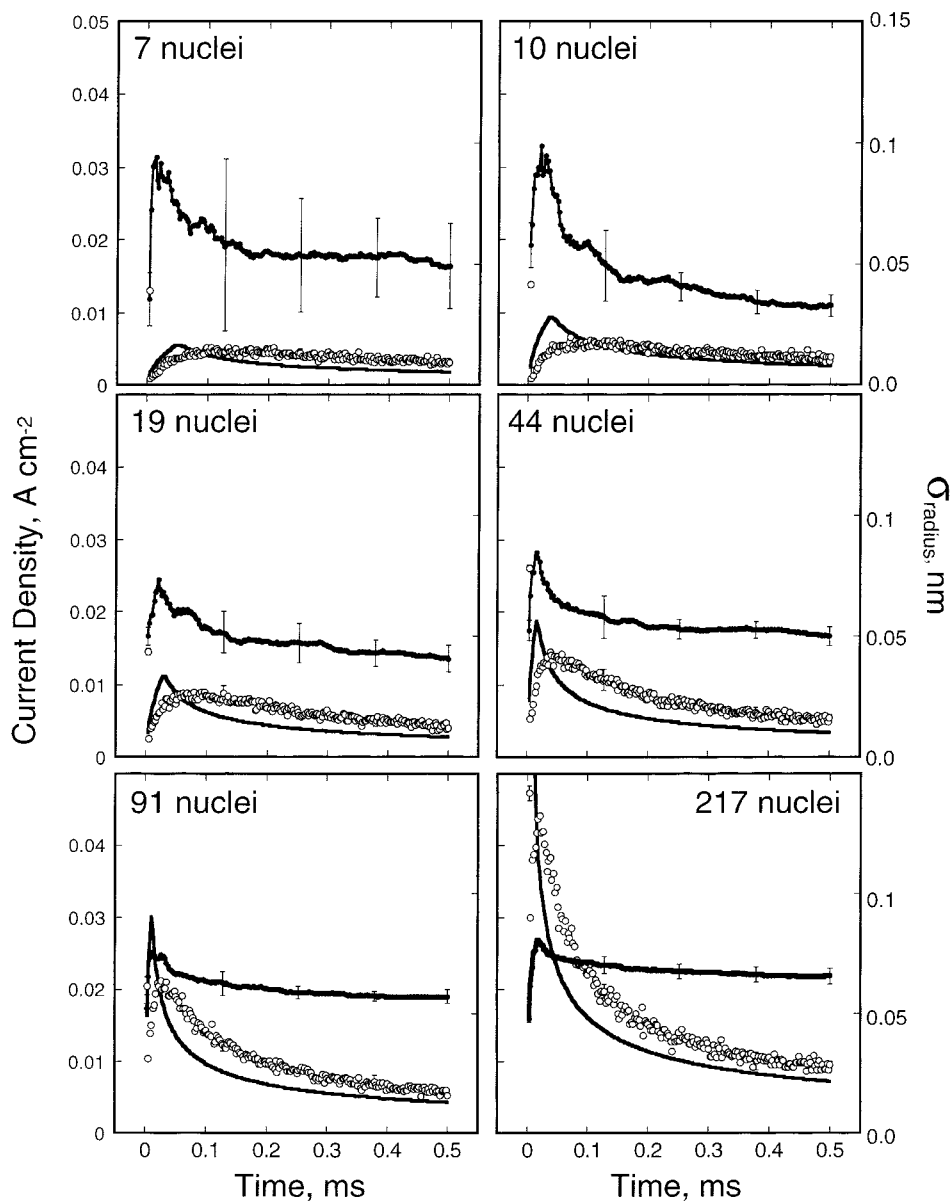


Figure 9. Current density (open circles) and the standard deviation of the particle radius, σ_R , (solid circles) as a function of time for *hexagonal arrays* and six nucleation densities. These BD simulation results represent the mean of three simulations, each of which involved a different silver plating solution. The standard deviation in the current and σ_R are indicated by the error bars ($\pm 1\sigma$). Data sets are labeled with the nucleation density in units of 10^9 cm^{-2} .

A quantitative comparison of the simulation data with the predictions of these equations is not possible because, as already mentioned, the area of the hexagonal domain (implicit in N_0 and $j(t)$ in eq 7) and the total geometric electrode area (implicit in $j(t)$ in eq 9) are not the same for our hexagonal ensembles because the hexagonal array does not cover the entire electrode surface. We have nevertheless attempted a comparison by using as the electrode area in eqs 7–9 the area covered by active (nonguard) nuclei in these arrays. In this case, $N_0 = 2/(\sqrt{3}d^2)$, where d is the distance between adjacent nuclei. This approximation permits a comparison of the t_{peak} between the simulation and eqs 7–9 (Figure 9, dashed line) but it leads to a calculated Cottrellian current in eq 9 which is too low. When we calculate the current transient using this assumption, two disparities between the calculated and the simulated current transients are observed: First, t_{peak} occurs at later times in the simulation current transients, and second, the simulation current density at short times—near t_{peak} —is significantly smaller than

is predicted by eqs 7–9. The elucidation of the reasons for this disagreement will provide a motivation for further study.

Again the solid circles in Figure 9 trace the evolution of the standard deviation of the particle radius, σ_R , as a function of deposition time. As compared with the data of Figure 4 for random ensembles, the main difference lies in the behavior of σ_R for $t > t_{\text{peak}}$, where σ_R no longer increases with time at any nucleation density. Plots of σ_R and $\sigma_R/\langle R \rangle$ versus $\langle R \rangle$ for these data shown in Figure 10 show that—in contrast to random ensembles of nanoparticles (compare with Figure 6)—low nucleation densities do not correlate with improved size monodispersity. In other words, excellent size monodispersity should be achievable for hexagonal arrays at any nucleation density even when the growth of adjacent nanoparticles on the surface is strongly coupled. These data confirm that the spatial inhomogeneity of the nucleation density is the primary source of particle size dispersion in experiments in which nanoparticles are grown under diffusion control on surfaces.

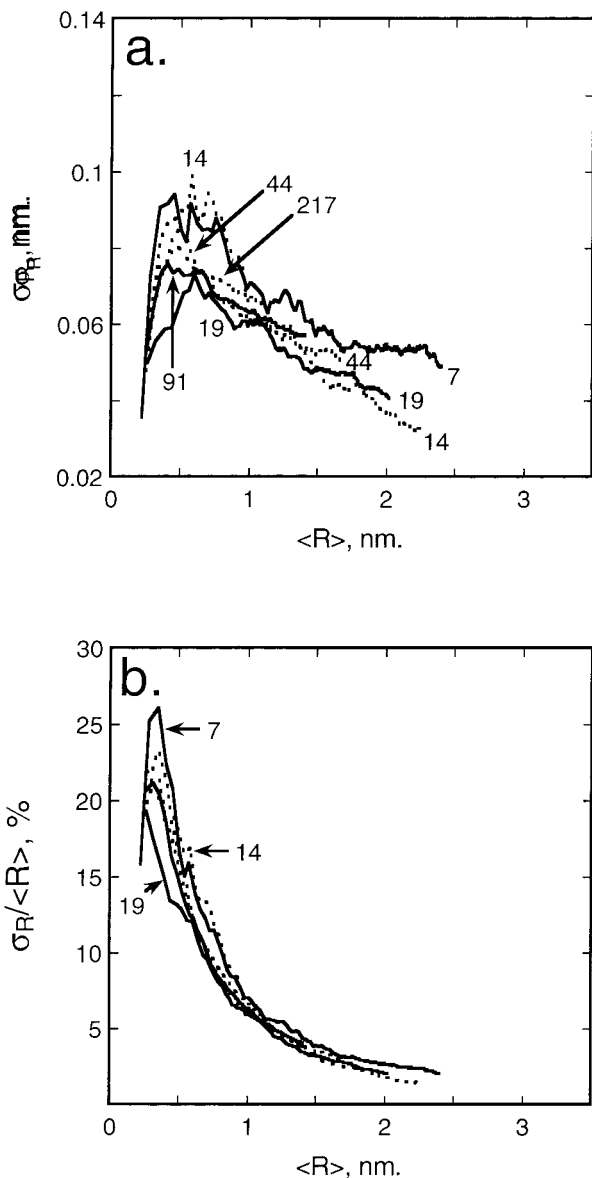


Figure 10. Plots of σ_R (a) and $\sigma_R/\langle R \rangle$ (b) as a function of $\langle R \rangle$ for the simulation data of Figure 9 (i.e., hexagonal arrays). Both σ_R and $\sigma_R/\langle R \rangle$ (see inset) decrease as a function of time following a rapid, initial increase in both quantities at short times.

Particle radius distributions are shown in Figure 11 for the 200 particle random ensemble (Figure 11a), and the 217 particle hexagonal array (three simulations each). These distributions, which are similar in shape to those obtained at lower particle areal densities, are skewed and exhibit a tail on the low R side. This distribution asymmetry was also seen in a previous simulation study²⁹ of nanoparticle growth for square arrays of nuclei. In that work, Bobbert et al.²⁹ used the mean field approximation to account for microscopic fluctuations in the diffusion field about each particle. The widths of the distributions shown in Figure 11 are similar to those reported by Bobbert. For example, for silver deposition at a nucleation density of $2 \times 10^{11} \text{ cm}^{-2}$ (comparable with the data of Figure 11), Bobbert²⁹ reported $\sigma_R/\langle R \rangle$ values of 4% and 6% at deposition times of 3 and 15 ms, respectively.

Although hexagonal arrays and random ensembles exhibit dramatically different behavior at long times, it is important to note that the evolution of σ_R at shorter times, $t \leq t_{\text{peak}}$, for these two types of nanoparticle ensembles is *identical*. We discuss the origin of this evolution of σ_R next.

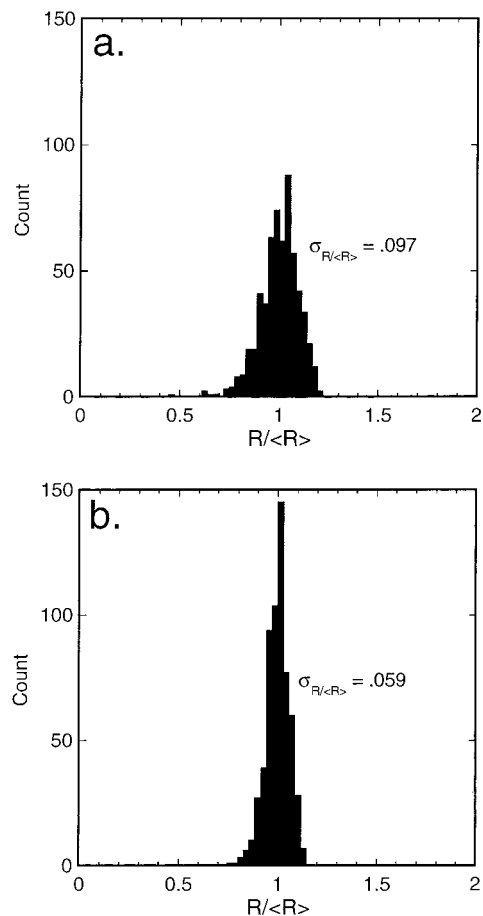


Figure 11. Representative particle size histograms for the 200 nuclei random ensemble and the 217 nuclei hexagonal arrays. All particles in three separate BD simulations (600 and 651, respectively) are tallied in these distributions.

C. The Reason for Size Distribution Narrowing for $t < t_{\text{peak}}$. Both random and hexagonal ensembles of nanoparticles exhibit a rapid increase in σ_{radii} at the onset of deposition followed by a decrease in σ_{radii} which continues until t_{peak} . What is the origin of this “size dispersion transient”?

The increase of σ_R and its subsequent decrease are both a consequence of the fact that the number of ions in the vicinity of a particular nucleus is a stochastic variable. Thus, the number of ions that arrive at a nucleus at the onset of deposition will depend on the number which happened to be in the immediate proximity of that nucleation site when deposition starts. This number will fluctuate about a mean value that is fixed by the concentration of silver ions in the solution. Because a very small volume of solution (i.e., number of silver ions) is “sampled” by each nucleus at short times, σ_R increases at the beginning of the simulation. As the deposition process continues and the diffusion field moves away from each nucleus, the volume of solution (and hence the number of ions) which is sampled around each nucleus increases and, concurrently, the number of atoms in each nucleus becomes more similar. This brings about the size distribution narrowing which is seen in all of the simulations of Figures 4 and 6 prior to t_{peak} .

This qualitative description can be made quantitative as follows: We assume that the number of atoms, N , in the growing nucleus is given by

$$N(t) = 2\pi C_{\text{Ag}^+} N_A \int_{a_0}^{\infty} r^2 P(r,t) dr \quad (10)$$

where N_A is Avogadro's number, a_0 is the radius of the nucleus at $t = 0$ (i.e., the critical nucleus size), and $P(r)$ is the probability that an ion initially at a distance r from the center of each particle will reach the surface of the growing nucleus by diffusion after a time t . This probability can be found from

$$P(r) = \begin{cases} 1 - 2\pi \int_a^{\infty} r'^2 p(r, r', t) dr' & \text{if } r \geq a \\ 1 & \text{if } r < a \end{cases} \quad (11)$$

where:

$$p(r, r', t) = \frac{1}{8\pi r r' \sqrt{\pi D_{Ag^+} t}} [e^{-(r-r')^2/4D_{Ag^+} t} - e^{-(r+r'-2a)^2/4D_{Ag^+} t}] \quad (12)$$

is the probability of finding an ion at a distance, r , and a time, t , that was initially at $r = r'$ when there is a perfectly absorbing barrier at $r = a$.³⁰ It is known that the number of ions, i , in a small volume of solution has a Poisson distribution.³¹ Because the number of atoms N in a nucleus is obtained through an importance sampling of a random variable, N (cf. eq 10), which has the same Poisson distribution everywhere inside the solution, the number of atoms N which make up a nucleus is also Poisson distributed with mean, N :

$$f_i(N) = e^{-N} \frac{N^i}{i!} \quad (13)$$

Hence the standard deviation σ_N of N is given by \sqrt{N} . The radius of the nucleus, R , is related to the number of atoms N inside the nucleus as

$$a = \sqrt[3]{a_0^3 + \frac{3M_{Ag}}{2\pi\rho_{Ag}N_A} N} \quad (14)$$

If σ_x is the standard deviation of a random variable, x , then the standard deviation of ax^b , where a and b are constants, is given by $abx^{b-1}\sigma_x$. Hence, the standard deviation of the radius of the nucleus is

$$\sigma_a = \frac{1}{3} \left[a_0^3 + \frac{3M_{Ag}}{2\pi\rho_{Ag}N_A} N \right]^{-2/3} \sqrt{(3a_0^3\sigma_{a_0})^2 + \left(\frac{3M_{Ag}}{2\pi\rho_{Ag}N_A} \sigma_N \right)^2} \quad (15)$$

This is approximately equal to:

$$\begin{aligned} \sigma_a &\approx \frac{1}{3} \sqrt[3]{\frac{3M_{Ag}}{2\pi\rho_{Ag}N_A} N}^{-2/3} \sigma_n \\ &\approx \frac{1}{3} \sqrt[3]{\frac{3M_{Ag}}{2\pi\rho_{Ag}N_A} N}^{-1/6} \end{aligned} \quad (16)$$

Thus, the standard deviation of the radius is predicted to decrease according to $n^{1/6}$. This analysis is valid for nuclei containing a minimum of five atoms; for a smaller number of atoms the Poisson distribution must be replaced by a Bernoulli distribution.

In Figure 12, the prediction of eq 16 is compared with σ_R as a function of $\langle n \rangle$ (the mean aggregation number) for the simulation of five randomly nucleated particles. This particular simulation data set is chosen because the mean internucleus distances are the largest (see Figure 2) and interactions between adjacent nuclei at short times can be expected to be the weakest. Good agreement is seen with the five particle data sets for $\langle N \rangle$

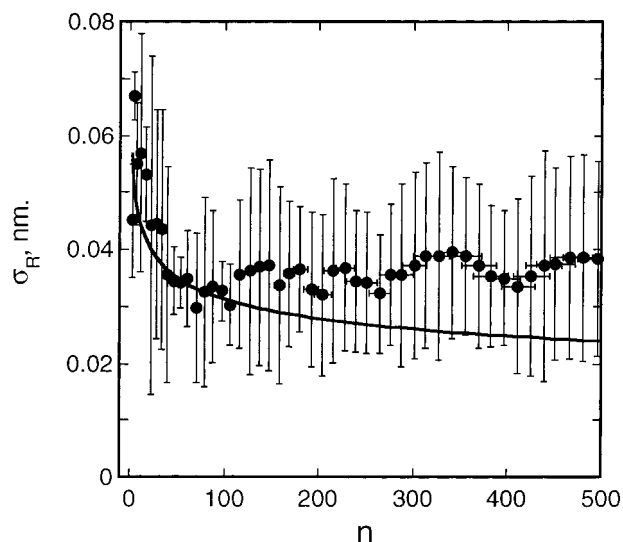


Figure 12. Plots of σ_R versus the aggregation number, n , which compare the predictions of eq 16 (solid lines) with BD results for single particle simulations (a) and for the five particle random ensembles (b). Results for three BD simulations were pooled to obtain the solid data points in both (a) and (b). Vertical error bars in (b) indicate the standard deviation of σ_R for these three data sets. Horizontal error bars in both (a) and (b) indicate the dispersion of n about the mean for the three simulations.

less than 150: Both the absolute magnitude of the simulation σ_R , and its initial rate of decrease are consistent with the predictions of eq 16. For larger values of $\langle N \rangle$ (i.e., longer deposition times), the standard deviation increases as a consequence of the flux inhomogeneities caused by the overlap of the diffusion fields as discussed earlier. For the other simulation data sets (both random and hexagonal) for larger numbers of nuclei, the simulation σ_R was consistently larger by a factor of 1.2–2 compared with the predictions of eq 16. This disparity is caused, in part, by the effects of diffusion layer overlap at short times—in advance of t_{peak} .

Summary

In this paper we have applied the BD method to investigate the growth of metal nuclei under conditions of diffusion control and instantaneous nucleation.

The data support the following conclusions:

(1) Three distinct temporal regimes—with respect to the evolution of size dispersion—exist in the growth of metal nanoparticles: (i) At short times ($t < 20$ ns), the standard deviation of the particle radius, σ_R , rapidly increases to 0.05–0.1 nm. (ii) At intermediate times in the interval from 20 to 200 ns, σ_R peaks and begins to decrease—nearly to zero in some experiments. This “convergent” growth segment continues until overlap of the diffusion fields of adjacent nanoparticles on the surface is nearly complete. (iii) At the longest times investigated in this study ($t > 0.2 \mu\text{s}$), the behavior of random and hexagonal ensembles diverge: Random ensembles again transition into a divergent growth regime in which σ_R increases monotonically with time; the size dispersion of hexagonal arrays, however, continues to decrease with deposition time.

(2) The size dispersion “transient” which occurs in time regimes (i) and (ii) above can be quantitatively understood in terms of the stochastic character of the deposition process. An analytical expression for σ_R vs N (eq 16) that predicts $\sigma_R \propto N^{-1/6}$ is in good agreement with the BD simulation results.

(3) In time regime (iii), the disparity that is seen in the simulation results for random ensembles and hexagonal arrays

proves that the increase in size dispersion that is seen for random arrays is caused by the inhomogeneous distribution of interparticle distances which translates into an inhomogeneity in the diffusion-limited flux at each particle. In essence, the growth law at each nanoparticle on the surface is different. This is the major difference between the growth of stationary particles on surfaces, and growth of diffusing colloid particles in solution: In solution, it can be assumed that the time-averaged growth law for each particle is identical.

(4) For random ensembles of nuclei, the width of the particle size distribution decreases as the nucleation density decreases. The onset of deleterious interparticle interactions (i.e., temporal regime (iii)) is delayed as the mean interparticle distance increases. This outcome is exactly that predicted by Ngo and Williams⁸ for the growth of particles on surfaces from gas-phase reactants.

Two additional points are worth making. First, for the growth of metal particles on surfaces, it has commonly been assumed that a broad distribution of nanoparticle sizes implies that nucleation is progressive. The simulation data presented here clearly proves that even when nucleation is truly instantaneous, particle size dispersion *will* develop, provided nuclei are randomly positioned on the surface, and grow at diffusion control.

Second, it is important to recognize that the existence of temporal regime (ii) in the growth curves of Figure 4 suggests a strategy for reducing size polydispersity in randomly nucleating systems: Nanoparticles are grown using a series of short deposition voltage pulses which are separated by much longer "decoupling" intervals during which the solution near the electrode surface is permitted to mix by diffusion. Compared with an experiment in which nanoparticles are grown in a single plating pulse, the size monodispersity of ensembles obtained using this "multipulse" approach will improve because a convergent growth segment will be introduced multiple times (i.e., at the beginning of each bias pulse) into the growth of a particle. We are currently investigating this hypothesis experimentally.

In addition to providing the specific insights discussed above, this study has demonstrated the strengths of the BD simulation method for investigating stochastic processes at electrode surfaces, and for investigating the various other mechanisms which are responsible for the development of inhomogeneity in electrodeposits. We are hopeful that BD will provide a powerful methodology for investigating a wide variety of other issues in electrochemistry including compositional inhomogeneities (in experiments in which multiple materials are co-deposited), activation-controlled electrodeposition, progressive nucleation processes, and transport irregularities at nanoscopic electrodes.

Acknowledgment. The authors thank Professor Benjamin Scharifker of the Simon Bolivar University (Caracas, Venezuela)

for supplying eqs 7–9 to us in advance of publication, and for valuable discussions. This work was supported by the Petroleum Research Fund of the American Chemical Society and by the National Science Foundation. R.M.P. gratefully acknowledges the following additional sources of funds: The NSF Young Investigator's Program (DMR-9257000), and an A.P. Sloan Fellow, an Arnold and Mabel Beckman Young Investigator award, and a Camille Dreyfus Teacher-Scholar award. R.M.P. also thanks Prof. A. J. Shaka of UCI for suggesting the Brownian dynamics method for investigating electrochemical nanoparticle growth. J.F. wishes to thank the FWO-Vlaanderen for a postdoctoral fellowship.

References and Notes

- (1) Klimenkov, M.; Nepijko, S.; Kühlenbeck, H.; Bäumer, M.; Schlögl, R.; Freund, H.-J. *Surf. Sci.* **1997**, *391*, 27.
- (2) Bäumer, M.; Frank, M.; Libuda, J.; Stempel, S.; Freund, H.-J. *Surf. Sci.* **1997**, *391*, 204.
- (3) "Dimensional uniformity" and "size monodispersity" applied to the particle diameter refer to the proximity of the relative standard deviation of the particle diameter (RSD_{dia}); the ratio of the mean diameter to the standard deviation of the diameter) to zero.
- (4) "Meso-scale" will refer to a critical dimension in the range from 10 Å and 1.0 μm .
- (5) Zoval, J. V.; Lee, J.; Gorer, S.; Penner, R. M. *J. Phys. Chem.* **1998**, *102*, 1166.
- (6) Zoval, J. V.; Stiger, R. M.; Biernacki, P. R.; Penner, R. M. *J. Phys. Chem.* **1996**, *100*, 837.
- (7) Stiger, R.; Craft, B.; Penner, R. M. *Langmuir* **1999**, *15*, 790.
- (8) Ngo, T. T.; Williams, R. S. *Appl. Phys. Lett.* **1995**, *66*, 1906.
- (9) "Temporally discrete" nucleation refers to a separation in time between the nucleation and growth phases of particle formation.
- (10) Sugimoto, T. *Adv. Colloid Interface Sci.* **1987**, *28*, 65.
- (11) Reiss, H. *J. Chem. Phys.* **1954**, *19*, 482.
- (12) LaMer, V. K.; Dinegar, R. H. *J. Am. Chem. Soc.* **1950**, *72*, 4847.
- (13) "Instantaneous" nucleation refers to a situation in which the time interval during which nucleation occurs is much shorter than the subsequent particle growth phase.
- (14) Ermak, D. L.; McCammon, J. A. *J. Chem. Phys.* **1978**, *69*, 1352.
- (15) Feldberg, S. W.; Auerbach, C. *Anal. Chem.* **1964**, *36*, 505.
- (16) Feldberg, S. W. *J. Am. Chem. Soc.* **1966**, *88*, 390.
- (17) Feldberg, S. W. *J. Phys. Chem.* **1966**, *70*, 3928.
- (18) Feldberg, S. W. *Electroanal. Chem.* **1969**, *3*, 199.
- (19) Cammarata, V.; Talham, D. R.; Crooks, R. M.; Wrighton, M. S. *J. Phys. Chem.* **1990**, *94*, 2680.
- (20) Li, W.; Hsiao, G. S.; Harris, D.; Nyffenegger, R. M.; Virtanen, J. A.; Penner, R. M. *J. Phys. Chem.* **1996**, *100*, 20103.
- (21) Nyffenegger, R. M.; Penner, R. M. *J. Phys. Chem.* **1996**, *100*, 17041.
- (22) Nagy, G.; Denault, G. *J. Electroanal. Chem.* **1997**, *433*, 175.
- (23) Fletcher, S. *J. Chem. Soc., Faraday Trans. 1* **1983**, *79*, 467.
- (24) Scharifker, B.; Hills, G. *Electrochim. Acta* **1983**, *138*, 225.
- (25) Marsaglia, G.; Narasimhan, B.; Zaman, A. *Comput. Phys. Commun.* **1990**, *60*, 345.
- (26) Scharifker, B.; Hills, G. *J. Electroanal. Chem.* **1981**, *130*, 81.
- (27) Bard, A. J.; Faulkner, L. R. *Electrochemical Methods: Fundamentals and Applications*; John Wiley and Sons: New York, 1980.
- (28) Scharifker, B. R., personal communication, Sept. 1998.
- (29) Bobbert, P. A.; Wind, M. M.; Vlieger, J. *Physica A* **1987**, *146*, 69.
- (30) Carslaw, H. S.; Jaeger, J. C. *The Conduction of Heat in Solids*, 2nd ed.; Oxford University Press: New York, 1959.
- (31) Chandrasekhar, S. *Rev. Mod. Phys.* **1943**, *15*, 1.